JMEPEG (2015) 24:1649–1655
DOI: 10.1007/s11665-015-1432-2

1059-9495/$19.00

Corrosion Behavior of Mg-6Al-1Zn+XRE Magnesium Alloy with Minor Addition of Yttrium

S. Manivannan, S.P.Kumaresh Babu, and Srinivasan Sundarrajan

(Submitted July 14, 2014; in revised form December 16, 2014; published online February 18, 2015)

The effect of yttrium addition on the microstructure of Mg-6Al-1Zn alloy was investigated by optical microscopy, x-ray diffraction analysis, and scanning electron microscopy. The experimental alloys were prepared by melting high-purity Mg, Al, Zn, and Y, respectively. Melting was carried out in a Inconel 718 crucible under SF_6 and ultra pure Ar (99.999%) gas mixture environment using electric arc furnace. The corrosion behavior of Mg-6Al-1Zn+*x*Yttrium (*x* = 0.5, 1.0 and 1.5 wt.% Y) magnesium alloy with different levels of yttrium additions was studied in 3.5 wt.% NaCl solution. Microstructure of yttrium-added alloy shows that higher grainrefinement is obtained in Mg-6Al-1Zn+0.5wt.%Y. Increasing yttrium content reduces the size of α-grain and alters the distribution of the β-phase ($Mg_{17}Al_{12}$) from continuous network morphology to small and dispersive distribution. It forms secondary intermetallic phase Al_2Y which has high melting point along the grain boundary. The corrosion resistance of Mg-6Al-1Zn magnesium alloy improved with addition of Yttrium. It was confirmed by the results of electrochemical polarization test. Based on the polarization curves, it is seen that fine precipitates of Al-Y intermetallic phase in Mg-6Al-1Zn alloy decrease the corrosion current density, thereby improving the corrosion resistance of the Mg-6Al-1Zn magnesium alloy.

Keywords corrosion, grainrefinement, magnesium alloy, microstructure, polarization

1. Introduction

Magnesium and magnesium alloys are attractive for microelectronics, automobile, and aircraft engine applications due to their low density, good damping characteristics, good thermal conductivity, and high-specific elastic modulus (Ref 1). However, use of magnesium and magnesium alloys is limited to structural and nonstructural components served in mild environments (Ref 2, 3). As magnesium alloys are finding new applications, challenges lie ahead in improving their high temperature strength and resistance to corrosion (Ref 4). Recent studies have concentrated on anodizing, ion implantation, laser direct melting, plasma electrolysis, and other surface modification techniques (Ref 5). These techniques help in protecting the surface of the alloys, and it is also necessary to improve the overall properties (corrosion and high temperature strength) of Mg alloys (Ref 6, 7). Improving these properties will ensure the longevity of the alloys even after the surface coating is damaged. Due to the presence of multiphase structure, magnesium alloy suffers from localized corrosion (galvanic effect). The high corrosion resistance exhibited by Mg-RE alloys can be attributed to the formation of less cathodic intermetallic compounds (Ref 8). Corrosion resistance of magnesium alloy has improved with increasing Al content up to 6.0 wt.% (Ref 9, 10). Many researchers have reported that the addition of rare earth elements, such as Y, La, Ce, Nd, and Gd are effective in improving the mechanical properties and corrosion resistance of Mg alloys (Ref 11-14). Yttrium is considered a more effective alloying element which improves the properties, especially the elevated temperature mechanical properties, of magnesium alloy compared to other RE elements (Ref 15, 16). More stable and chemically less reactive hydroxide protective film was formed on alloying yttrium with magnesium, resulting in higher corrosion resistance in pure water (Ref 17). Many investigations have been carried out on the effect of RE addition on corrosion behavior of AZ91D magnesium alloys, and the effect of yttrium addition is still unexplored fully in Mg-6Al-1Zn magnesium alloy. In the present study, the effect of yttrium addition to Mg-6Al-1Zn alloy, as a grain refiner and its effects on alloy's corrosion behavior when subjected to chloride environment, was extensively studied.

2. Experimental Procedures

The material used in this study was an AZ61 magnesium alloy with composition of Mg-6Al-1Zn. The commercial Mg and Mg-Y Master alloy obtained from China Shanxi Xinghua Cun International Trading Co. (China), and commercial Al and Zn are obtained from Johnson Matthey Chemicals India Pvt. Ltd. (India). The chemical compositions of the experimental alloys were confirmed using AES spectroscopy methods, and results are listed in Table 1. Commercially pure Mg, Al and Zn were weighed and added to the crucible. Predetermined amounts of Mg-Y master alloys were carefully weighed and added to the melt at 720 °C with the continued supply of gas mixture consisting of 99.5% Ar and 0.5% SF_6 at the rate of

S. Manivannan and **S.P. Kumaresh Babu**, Department of Metallurgical and Materials Engineering, National Institute of Technology, Tirchirappalli 620 015 Tamil Nadu, India; and **Srinivasan Sundarajan**, National Institute of Technology, Tirchirappalli 620 015 Tamil Nadu, India. Contact e-mails: manivannan.meta@gmail.com, babu@nitt.edu, and sundar@nitt.edu.

Table 1 Chemical composition of Mg-6Al-1Zn-XRE (in wt.%)

Alloy	Al	Mn	Zn	Si	Cu	Ni	Fe	Mg
AZ61+0.0Y	5.8	0.02	0.4	0.1	0.05	0.05	0.005	Bal.
AZ61+0.5Y	5.73	0.15	0.33	0.07	0.05	0.03	0.005	Bal.
AZ61+1.0Y	5.85	0.08	0.52	0.15	0.01	0.02	0.04	Bal.
AZ61+1.5Y	5.63	0.10	0.80	0.18	0.1	0.03	0.004	Bal.

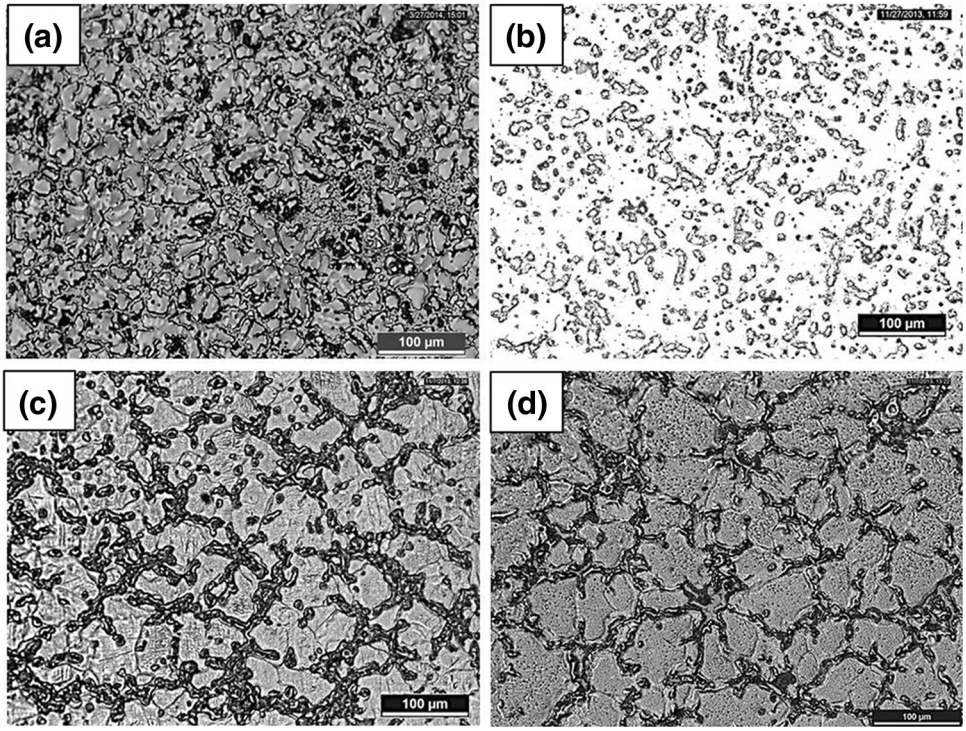

Fig.1 As-cast Microstructure of Mg-6Al-1Zn alloy. (a) 0.0 wt.% Y. (b) 0.5 wt.% Y. (c) 1.0 wt.% Y. (d) 1.5 wt.% Y

0.25 m^3/h. The cast specimens were cold mounted, polished with SiC emery papers staring from 80 to 2000 grit size, and diamond polished up to 1 micron. The polished specimens were etched using 2.0 wt.% Nital solution for 5-10 s to perform optical microscopy (OM). The microstructure of the cast specimens was obtained using DIC Leica OM, Model No: DM750M. The effects of grainrefinement of α-phase and size of β-phase for refined and un-refined alloys were also observed using Hitachi Scanning Electron Microscopy (SEM) equipped with energy-dispersive spectrometers (EDS). Phases were confirmed using x-ray diffraction technique. Immersion tests were conducted to evaluate the corrosion rate of samples through weight loss method with ASTM G31-72. The corrosion test specimens were evaluated as per ASTM G1-03 standard. The corrosion behavior of yttrium-added alloy was experimented in 3.5% NaCl environment. The electrochemical corrosion measurements were carried out in a three-electrode setup using GillAC electrochemical corrosion analyzer, cell containing about 500 ml of Mg $(OH)_2$ saturated 3.5 wt.% NaCl solution. Saturated calomel electrode used as a reference with a platinum electrode as counter and a sample as the working electrode. The electrochemical polarization tests were done in triplicate. The surface topography of the exposed specimens was further investigated by microscopy techniques.

Table 2 Fraction of alpha and beta plus RE Phases in Mg-6Al-1Zn-XRE (in wt.%)

Experimental alloy	Alpha phase	Beta phase + RE phases
Mg-6Al-1Zn	60.99	32.45
Mg-6Al-1Zn+0.5Y	78.67	23.97
Mg-6Al-1Zn+1.0Y	61.31	38.72
Mg-6Al-1Zn+1.5Y	62.35	33.27

3. Results and Discussion

3.1 Effects of Yttrium on Mg-6Al-1Zn Magnesium Alloy

The microstructure of the base material shown in Fig. 1(a) consists of α and β ($Mg_{17}Al_{12}$) phase in continuous network shape. The β-($Mg_{17}Al_{12}$) phase accelerates corrosion of magnesium alloy as a cathode owing to its higher corrosion

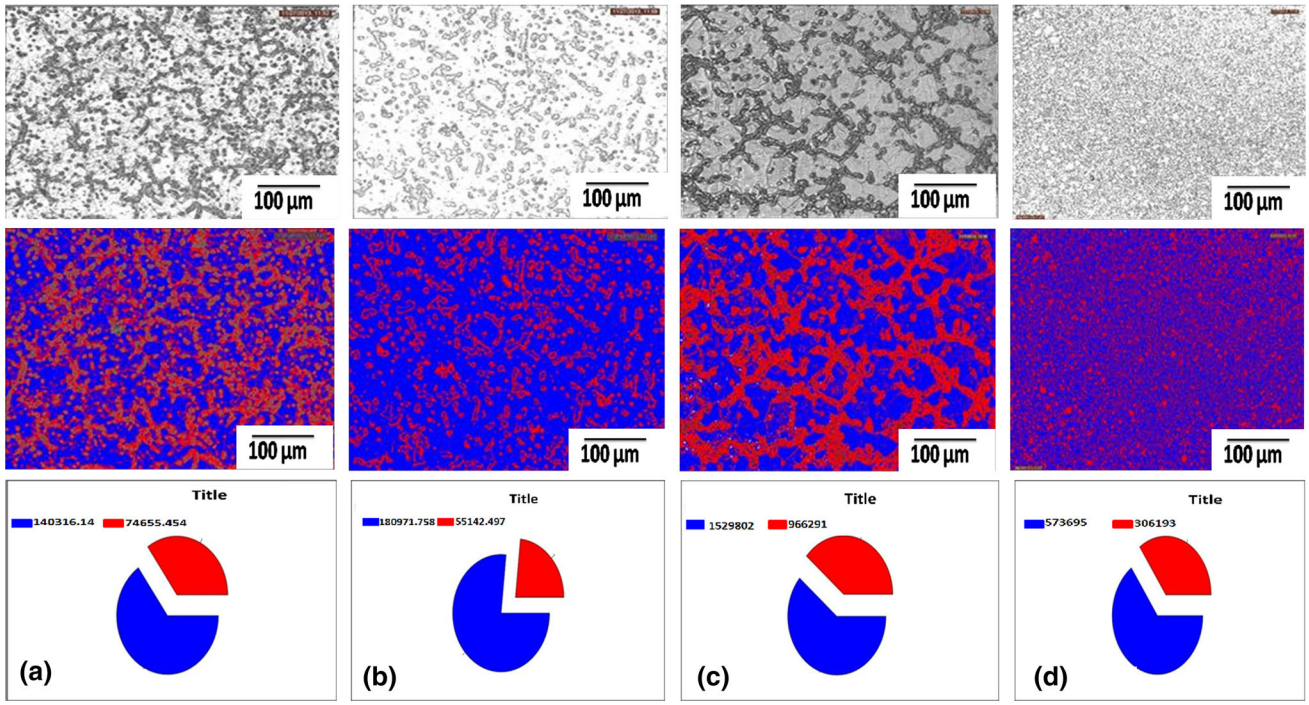

Fig.2 Phase analysis for Mg-6Al-1Zn. (a) 0.0 wt.% Y, (b) 0.5 wt.% Y, (c) 1.0 wt.% Y, and (d) 1.5 wt.% Y

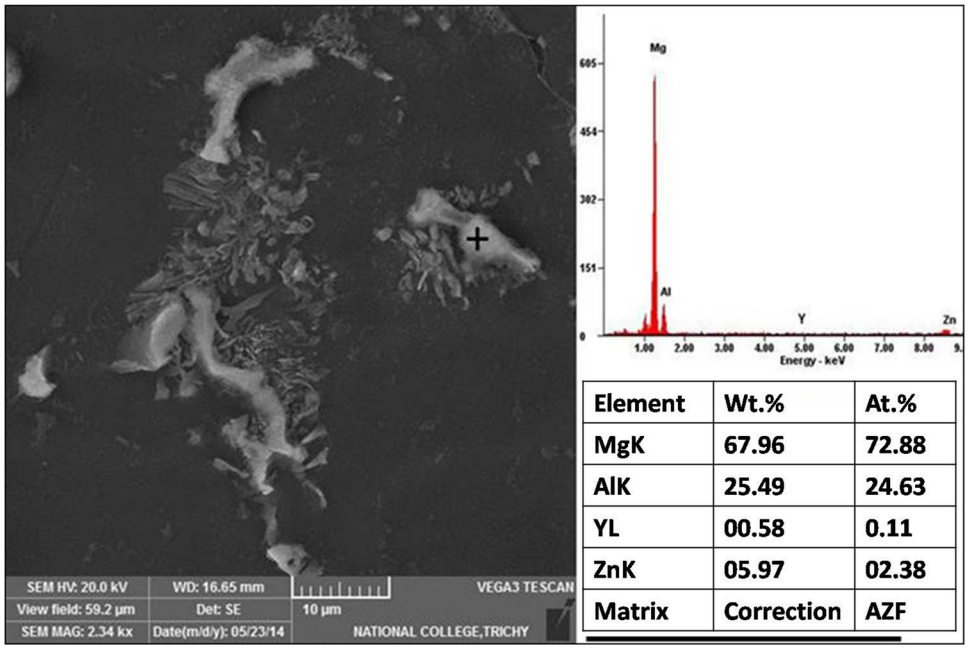

Fig.3 SEM and EDX analysis of Mg-6Al-1Zn+0.5wt.%Y

potential than that of the surrounding bulk material (α-Mg). The Mg-6Al-1Zn magnesium alloy is remarkably refined by yttrium, which is concentrated on the solid-liquid interface during solidification process, suppressing the growth of β-phase. The addition of 0.5 wt.% Y to Mg-6Al-1Zn results in the higher grainrefinement due to nucleation of Al_2Y intermetallic phase along the α matrix as shown in Fig. 1(b). As the addition of yttrium is increased from 0.5 to 1.0 wt.% and then to 1.5 wt.%, there is a corresponding increase in nucleation of Al_2Y intermetallic phase and higher isolation of β ($Mg_{17}Al_{12}$)

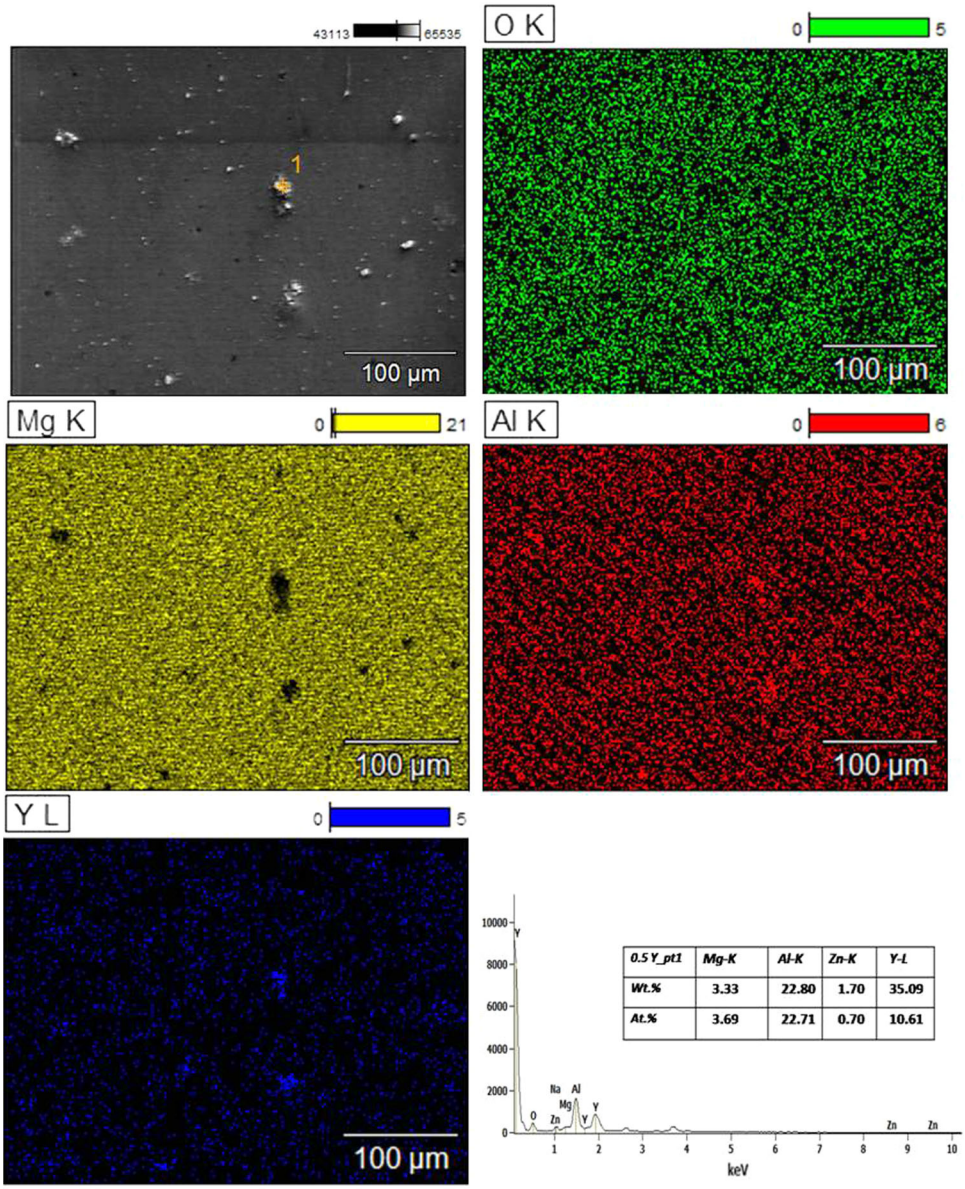

Fig.4 X-ray mapping of Mg-6Al-1Zn+0.5wt.%Y alloy sample showing the regions of Al-Y phase

phase. This is confirmed by the microstructures shown in Fig. 1(c) and (d). The higher wt.% yttrium has also resulted in lower volume fraction of β ($Mg_{17}Al_{12}$) as tabulated in Table 2 and Fig. 2.

3.2 SEM and EDX Analysis

Figure 3 shows the SEM analysis of Mg-6Al-1Zn+0.5 wt.%Y and EDS patterns of β-phase. The microstructure consists of α-phase surrounded by (α + β) eutectic lamellar precipitates and isolated β-phases. EDS analysis was performed on β-phase that confirms the formation of intermetallic $Mg_{17}Al_{12}$ and Al_2Y (Fig. 4). Alpha (anode) and beta (cathode) phases form micro-galvanic couples (Ref 18). After the addition of yttrium, cathodic effect is so weaker in β-$Mg_{17}Al_{12}$ phase side of the couple that couple itself is diminished. Phase analysis provided the information on the different phases in α-Mg and β-$Mg_{17}Al_{12}$ + RE phase fraction. This has been shown in different colors in Fig. 2. In addition, the Al_2Y phase emerges at the grain boundary, simultaneously the composition of typical Al-Mg phase changes.

3.3 X-ray Diffraction

Figure 5 shows the x-ray diffraction analysis (XRD) analysis of Mg-6Al-1Zn+XRE (where X = 0.0, 0.5, 1.0, and 1.5 wt.% Y) alloys. The XRD confirmed the α-phase, β-phase ($Mg_{17}Al_{12}$), and Al_2Y intermetallic phase present in these alloys. The pattern reveals that the β-phase ($Mg_{17}Al_{12}$) is a main microscopic element of the Mg-6Al-1Zn magnesium alloy. Due to the presence of yttrium in Mg-6Al-1Zn alloy, the

formation of high melting point intermetallic element Al_2Y along the α-magnesium matrix is promoted.

3.4 Density Test

Density of the experimented alloys was tested using Archimedes' principle and found that the density of an alloy containing 0.5 wt.% of yttrium and 1.5 wt.% of yttrium has decreased compared to that of base magnesium alloy (Mg-6Al-1Zn+0.0wt.%Y). This is due to the presence of intermetallics of Al_2Y and isolated β-phase ($Mg_{17}Al_{12}$). The density test results are given in Table 3.

3.5 Corrosion Test

3.5.1 Microstructure After Immersion Test. Figure 6 shows the optical microstructures of Mg-6Al-1Zn+xRE (where x = 0.0, 0.5, 1.0, and 1.5 wt.% Y) after immersion test in 3.5% NaCl Solution. In case of base alloy, the corrosion surfaces had two characteristics: one was the runaway of corrosion film from corrosion surface and the other was severe pitting corrosion. Mg-6Al-1Zn+0.5wt.%Y shows lower corrosion rate compared to the alloy containing 1.0 and 1.5 wt.% Y.

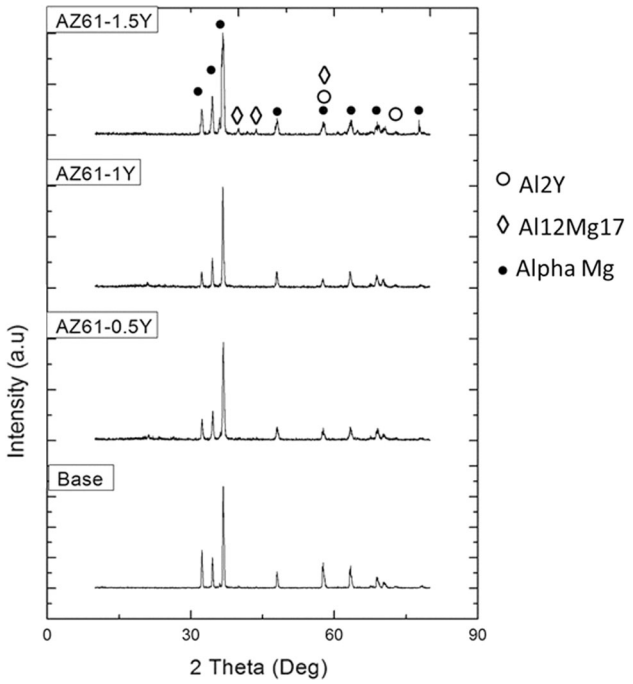

Fig.5 XRD analysis of Mg-6Al-1Zn+XRE

3.6 Corrosion Rate

The variation of corrosion rate of alloy with different contents of the rare earth element yttrium is shown in Fig. 7. The corrosion rate of the alloy with 0.5, 1.0, and 1.5 wt.% Y is considerably lower than that of base magnesium alloy. The results confirmed that addition of rare earth element (yttrium) has improved the corrosion resistance of Mg-6Al-1Zn magnesium alloy markedly. This significant improvement could be attributed to the new phases containing Mg-Y and Al-Y forming on the grain boundaries as well as in the grain interior. The Al-Y phase improves the film-forming tendency on the surface of β-phase ($Mg_{17}Al_{12}$), thus reducing the corrosion attack. However, with the increase of rare earth yttrium above 0.5 wt.% in Mg-6Al-1Zn magnesium alloy, the corrosion rate becomes slightly higher, and further addition of Y content over 1.0 wt.% results in the increment of the corrosion rate, which suggests that excessive addition of rare earth (yttrium) leads to reduced corrosion resistance of Mg-6Al-1Zn magnesium alloy. As Fig. 1 shows the change in microstructures, the addition of yttrium in magnesium alloy could increase the amount of β-phase ($Mg_{17}Al_{12}$) on the grain boundaries and help them to be more continuous manner. This might be a reason for lower corrosion resistance at higher yttrium addition.

3.7 Potentiodynamic Polarization Test

In the potentiodynamic polarization test, the applied potential is increased with time and the current is constantly monitored. The current density is plotted against the potential. From the polarization curves, the corrosion current (I_{corr}) was determined by Tafel extrapolation method. The polarization curves of base magnesium alloy and yttrium-added alloys are shown in Fig. 8(a). Yttrium addition to the Mg-6Al-1Zn magnesium alloy shifts the corrosion potential to positive gradually and makes the corrosion rate derived from corrosion current densities decrease. From the Tafel curve, it was noted that a large number of small alloying additions of yttrium can ennoble the E_{corr} value of Mg-6Al-1Zn magnesium alloy (Table 4). The alloy with 0.5 wt.% Y addition manifest the low corrosion rate as compared to 0.0, 1.0, and 1.5 wt.% of Y. It was clearly observed that yttrium additions on Mg-6Al-1Zn magnesium alloy have a potent tendency to raise the E_{corr} value. The above results agree fairly well with those obtained from the immersion test. The E_{corr} and I_{corr} values are listed in Table 4. Many researchers reported (Ref 19, 20) that β-phase distributed along α grain boundary acts as a micro-galvanic cathode. The current produced between β-phase and α-phase is micro-galvanic in nature. It mainly attacks α-phase resulting in corrosion of α grain due to which the β-phase is flaked away. Refinement of α- and β-phase results in the weakening of micro-galvanic corrosion. Yttrium addition has resulted in size reduction of primary α grain and β-phase. Also the area ratio of

Table 3 Corrosion Rate

Alloy	Weight loss, g	Density, g/cc	Area, cm^2	Time of exposure, h	Corrosion rate, mm/year	Standard deviation
Mg-6Al-1Zn+0.0wt.%Y	0.201	1.7770	7.8	72	17.64	0.1205
Mg-6Al-1Zn+0.5wt.%Y	0.004	1.7664	5.7	72	0.48	0.0208
Mg-6Al-1Zn+1.0wt.%Y	0.068	1.7762	6.3	72	7.4	0.1
Mg-6Al-1Zn+1.5wt.%Y	0.096	1.7264	3.66	72	18.50	0.1

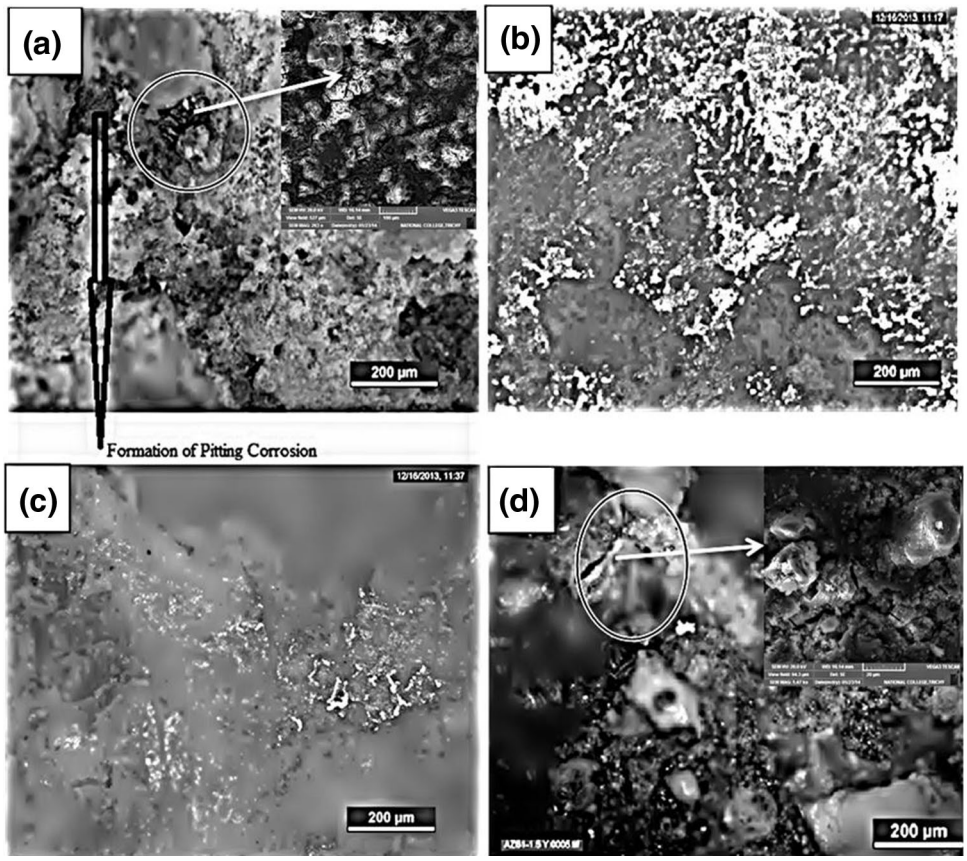

Fig.6 Optical microstructures of Mg-6Al-1Zn alloy after immersion test. (a) 0.0 wt.% Y. (b) 0.5 wt.% Y. (c) 1.0 wt.% Y. (d) 1.5 wt.% Y

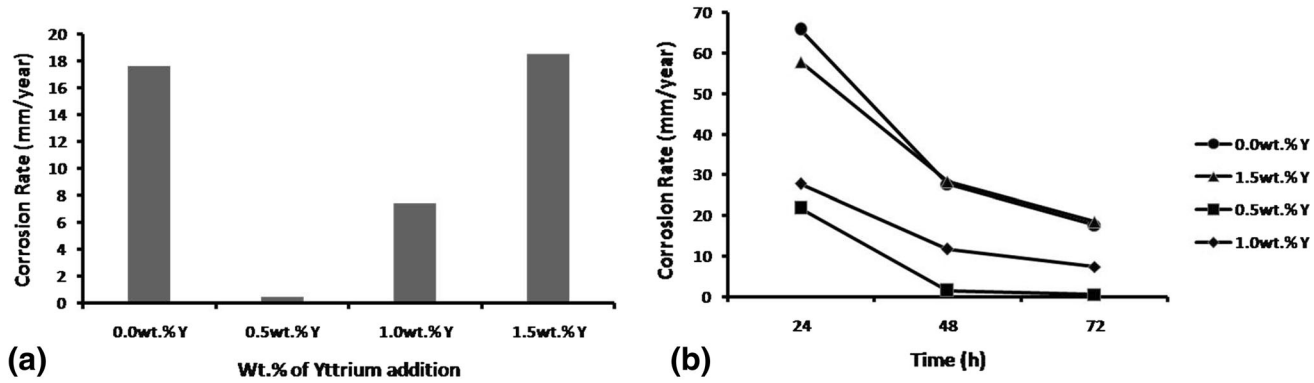

Fig.7 Average corrosion rates for the mass loss in 72 h for Mg-6Al-1Zn+XRE in 3.5 wt.% NaCl solution. (a) Corrosion rate vs. yttrium content (wt.%). (b) Corrosion rate vs. time (in h)

β phase to adjacent α grain decreases. It is noted that solid solution of aluminum in α-phase benefits reducing corrosion in α phase. This in turn declines the density between β-phases to adjacent α grain.

4. Conclusions

(1) Minor addition of yttrium to Mg-6Al-1Zn magnesium alloy causes significant refinement of microstructure including primary α-phase and eutectic (α + β) lamellar phase.
(2) The refined microstructure results in the remarkable improvement of corrosion resistance.
(3) Lower Icorr value was obtained in Mg-6Al-1Zn+ 0.5wt.%Y confirming the high corrosion resistance of this magnesium alloy compared to other alloys such as Mg-6Al-1Zn + 0.0, 1.0, and 1.5 wt.% Y.
(4) The corrosion resistance of the yttrium-added Mg-6Al-1Zn alloy has increased compared to that of the base Mg-6Al-1Zn magnesium alloy, due to the grainrefine-

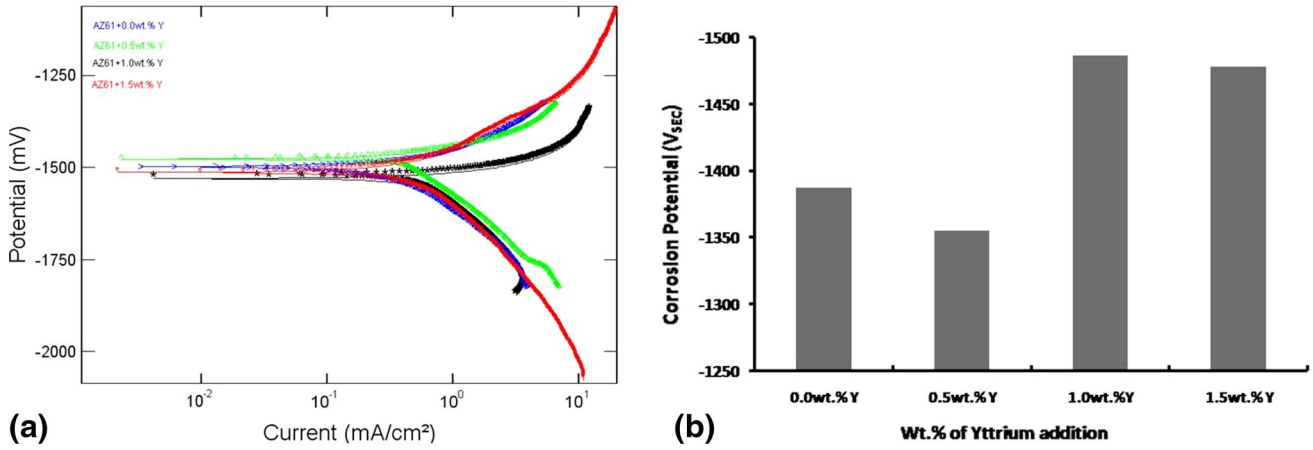

Fig.8 (a) Polarization curves of Mg-6Al-1Zn+XRE alloy in 3.5 wt.% NaCl solutions. (b) Effect of yttrium addition on corrosion potential

Table 4 Potentiodynamic polarization results

Alloy	E_{CORR}, mV	I_{CORR}, mA/cm^2	Corrosion rate, mm/year
AZ61+0.0wt.%Y	−1387.2	0.3432	7.8773
AZ61+0.5wt.%Y	−1355.1	0.1435	3.295
AZ61+1.0wt.%Y	−1486	1.0301	15.48
AZ61+1.5wt.%Y	−1477.7	0.2192	5.0318

ment of β-phase from continuous network morphology to small and dispersive distribution along the grain boundary by forming the secondary intermetallic Al_2Y phase.

The improvement in corrosion resistance of Mg-6Al-1Zn+*x*Yttrium alloy will increase the longevity of automotive engine blocks and in other fields where Mg-6Al-1Zn alloy is used.

References

1. S. Wang, Microstructure and Mechanical Properties of AZ91 Alloys by Addition of Yttrium, *JMEPEG*, 2009, **18**, p 137–144
2. E. Aghion and B. Bronfin, Magnesium Alloys Development Towards the 21st Century, *Mater. Sci. Forum*, 2000, **19**, p 350–351
3. S. Schumann and H. Friedrich, Current and Future Use of Magnesium in the Automobile Industry, *Mater. Sci. Forum*, 2003, **51**, p 419–422
4. G. Pettersella, H. Westengen, R. Høera, and O. Lohne, Microstructure of a Pressure Die Cast Magnesium 4 wt.% Aluminium Alloy Modified with Rare Earth Additions, *Mater. Sci. Eng. A*, 1996, **207**, p 115–120
5. Z. Yao, Y. Xu, Y. Liu, D. Wang, Z. Jiang, and F. Wang, Structure and Corrosion Resistance of ZrO_2 Ceramic Coatings on AZ91D Mg Alloys by Plasma Electrolytic Oxidation, *J. Alloys Compd.*, 2011, **509**, p 8469–8474
6. L.O. Snizhko, A.L. Yerokhin, A. Pilkington, N.L. Gurevina, D.O. Misnyankin, A. Leyland, and A. Matthews, Anodic Processes in Plasma Electrolytic Oxidation of Aluminium in Alkaline Solutions, *Electrochim. Acta*, 2004, **49**, p 2085
7. Y. Ma, X. Nie, D.O. Northwood, and H. Hu, Corrosion and Erosion Properties of Silicate and Phosphate Coatings on Magnesium, *Thin Solid Films*, 2004, **469-470**, p 472
8. F. Zucchi, Electrochemical Behaviour of a Magnesium Alloy Containing Rare Earth Elements, *J. Appl. Electrochem.*, 2006, **36**, p 195–204
9. G. Song and A. Atrens, Understanding Magnesium Corrosion, *Adv. Eng. Mater.*, 2003, **5**(12), p 837–858
10. D. Eliezer, P. Uzan, and E. Aghion, Effect of Second Phases on the Corrosion Behaviour of Magnesium Alloys, *Mater. Sci. Forum*, 2003, **419-422**, p 857–866
11. G.L. Song and D. Stjohn, The Effect of Zirconium Grain Refinement on the Corrosion Behaviour of Magnesium-Rare Earth Alloy MEZ, *J. Light Met.*, 2002, **2**(1), p 1–16
12. T. Takenaka, T. Ono, Y. Narazaki, Y. Naka, and M. Kawakami, Improvement of Corrosion Resistance of Magnesium Metal by Rare Earth Elements, *Electrochim. Acta*, 2007, **53**(1), p 117–121
13. J.H. Nordlien, K. Nisancioglu, S. Ono, and N. Masuko, Morphology and Structure of Water-Formed Oxides on Ternary MgAl Alloys, *J. Electrochem. Soc.*, 1997, **144**(2), p 461–466
14. F. Rosalbino, E. Angelini, S. De Negri, A. Saccone, and S. Delwno, Effect of Erbium Addition on the Corrosion Behaviour of Mg-Al Alloys, *Intermetallics*, 2005, **13**(1), p 55–60
15. M. Liu, The Influence of Yttrium (Y) on the Corrosion of Mg-Y Binary Alloys, *Corros. Sci.*, 2010, **52**, p 3687–3701
16. F. Wang, Effects of Combined Addition of Y and Ca on Microstructure and Mechanical Properties of Die Casting AZ91 Alloy, *Trans. Nonferr. Met. Soc. China*, 2010, **20**, p s311–s317
17. J. Zhang, X. Niu, X. Qiu, K. Liu, C. Nan, D. Tang, and J. Meng, Effect of Yttrium-Rich Misch Metal on the Microstructures, Mechanical Properties and Corrosion Behaviour of Die Cast AZ91 Alloy, *J. Alloys Compd.*, 2009, **471**, p 322–330
18. J.-X. Niu, Q.-R. Chen, N.-X. Xu, and Z.-L. Wei, Effect of Combinative Addition of Strontium and Rare Earth Elements on Corrosion Resistance of AZ91D Magnesium Alloy, *Trans. Nonferr. Met. Soc. China*, 2008, **18**, p 1058–1064
19. Y.L. Song, Y.H. Liu, S.H. Wang, S.R. Yu, and X.Y. Zhu, Effect of Cerium Addition on Microstructure and Corrosion Resistance of Die Cast AZ91 Magnesium Alloy, *Mater. Corros.*, 2007, **58**, p 189–192
20. G.L. Song, A.L. Bowles, and D.H. StJohn, Corrosion Resistance of Aged Die Cast Magnesium Alloy AZ91D, *Mater. Sci. Eng. A*, 2004, **366**, p 74–86